JOURNAL OF AIRCRAFT
Vol. 44, No. 1, January–February 2007

Implementing Time-Based Spacing for Decelerating Approaches

W. F. de Gaay Fortman,* M. M. van Paassen,† M. Mulder,‡ and A. C. in 't Veld§
Delft University of Technology, 2629 HS Delft, The Netherlands
and
J. P. Clarke¶
Georgia Institute of Technology, Atlanta, Georgia 30332-0150

DOI: 10.2514/1.22253

The three-degree decelerating approach is a promising noise abatement procedure shown to significantly reduce noise impact on communities surrounding airports. However, a limitation to a widespread implementation of this and other noise abatement procedures is that runway capacity is compromised. The reason for this is that air traffic controllers increase spacing between in-trail aircraft to compensate for the uncertainties in the descent trajectory. The research presented in this paper focuses on simplifying the task of the controller by requiring aircraft to accurately hit a required time of arrival over the runway. A key component in the development of the associated pilot support interface necessary to help pilots in their new task is a wind profile prediction algorithm that estimates the actual wind profile and predicts how it will evolve in time along the descent trajectory. Rather than using a boundary layer model for estimating the wind profile, the wind prediction algorithm uses historical wind measurement data from preceding aircraft. By incorporating the wind prediction algorithm in an advanced flap scheduler algorithm, accurate time-to-fly estimates can be made for the three-degree decelerating approach. Monte Carlo simulations were conducted to test the robustness of the algorithm and analyze the control space for various wind conditions. Maximum feasible deviations in terms of time while satisfying noise goals are shown to be between 8 and 30 s. The pilot support interface was designed and tested in a piloted experiment. Performance in terms of noise and time goals as well as workload is consistent and significantly better with respect to the nonsupported condition, for all wind conditions, but, in particular, for more complex wind conditions.

I. Introduction

SINCE the introduction of the jet engine in the early 1960s various solutions have been proposed to mitigate aircraft noise. Solutions have been sought in land zoning policies in the vicinity of airports, modifications to airframes and jet engines, and in noise abatement procedures, both for approaching and departing aircraft. Especially in the area of approach procedures there still are good opportunities for improvement. Presently, standard approach procedures are characterized by horizontal segments at low altitudes and low, constant speeds, requiring flight with an extended flap configuration and high throttle settings to offset the additional drag.

Various noise abatement procedures have been developed with the aim of minimizing the noise impact on communities during the approach trajectory [1–12]. The noise benefit of these procedures is mainly achieved by flying a higher approach path without level segments with low throttle settings and a clean configuration (no flaps and no landing gear). Figure 1 shows the obvious noise benefits of a three-degree decelerating approach (TDDA) compared to a standard instrument landing system (ILS).

Many barriers exist to the implementation of noise abatement procedures. These include pilot acceptance, conformance to present air traffic control (ATC) procedures, and effects on airport capacity. Studies at Schiphol Airport have shown that an ad hoc implementation of a continuous descent approach (CDA) reduced airport capacity by as much as 50% [3]. The underlying reason for this is that air traffic controllers are unable to adequately space aircraft decelerating at different rates and therefore apply larger than normal spacing buffers to ensure minimum separation. The variations in the aircraft deceleration rates are due to three factors. First, each aircraft type has its own lift–drag characteristics which determine its aerodynamic performance. Second, pilots are free to select flap and throttle settings at their own discretion. Third, meteorological conditions (i.e., wind speed and direction) affect the deceleration profile of the aircraft with respect to the ground.

As knowledge of the aircraft characteristics is more readily available in the cockpit rather than on the ground, this research proposes a scenario where the controller only assigns a required time of arrival (RTA) at a fix close to the runway and leaves it up to the pilots to meet this RTA. By providing the pilot with a support interface driven by a flap scheduler algorithm, the pilot is able to meet the RTA while flying an idle thrust three-degree decelerating approach, controlling his descent and speed profile solely by the timing of subsequent flap selections. Knowledge of the wind profile and its estimated future behavior along the approach trajectory alleviates the last of the three uncertainty factors in the noise abatement procedure, allowing the aircraft to consistently meet the RTA so that controllers can confidently sequence and space aircraft in the terminal maneuvering area (TMA) more tightly, ultimately increasing runway capacity.

The following results are discussed in this paper: 1) the characteristics of the TDDA, 2) the characteristics of the wind profile

Presented as Paper 6141 at the AIAA Guidance, Navigation, and Control Conference and Exhibit, San Francisco, California, 15–18 August 2005; received 4 January 2006; revision received 27 May 2006; accepted for publication 29 May 2006.

*Research Associate, Control and Simulation Division, Faculty of Aerospace Engineering, Kluyverweg 1.

†Associate Professor, Control and Simulation Division, Faculty of Aerospace Engineering, Kluyverweg 1; m.m.vanpaassen@tudelft.nl. Member AIAA.

‡Assistant Professor, Control and Simulation Division, Faculty of Aerospace Engineering, Kluyverweg 1; m.mulder@tudelft.nl. Member AIAA.

§Research Associate, Control and Simulation Division, Faculty of Aerospace Engineering, Kluyverweg 1; a.c.intveld@tudelft.nl. Member AIAA.

¶Associate Professor, School of Aerospace Engineering, 270 Ferst Drive NW; john-paul.clarke@ae.gatech.edu. Member AIAA.

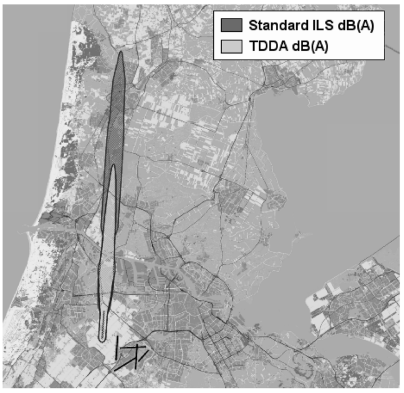

Fig. 1 The 65 dB(A) maximum noise level contours for a Boeing 747 approaching runway 18R at Schiphol Amsterdam airport. The noise footprint of the TDDA is much smaller than the standard ILS approach. Most of the noise benefits for the TDDA are the result of flying higher for longer. Note that under operational circumstances a straight-in approach is not standard.

in the TMA, 3) the design and incorporation of a wind prediction algorithm in a flap scheduler algorithm to improve the RTA performance of aircraft flying a TDDA under various wind conditions, 4) the results of a Monte Carlo simulation to test the effectiveness of the algorithm for various wind conditions, and 5) a piloted experiment in a six-degree-of-freedom research flight simulator to test the effectiveness of the proposed automation.

II. Three-Degree Decelerating Approach

A. Description of the Procedure

Based on a systems analysis of the noise reduction benefits of the two segment approach (TSA) and the TDDA relative to the conventional ILS approach, the TDDA was deemed to be the most promising noise abatement procedure that lies within the boundaries of present approach procedure limitations and can be implemented within a short time horizon [1]. During the TDDA, a curved or straight approach path at a 3 deg angle is created from any point using advanced navigation tools. Though different implementations are feasible, the TDDA presented in this paper has the following characteristic parameters: an aircraft intercepts the 3 deg glide path at 7000 ft at an airspeed of 250 kts. At a predetermined altitude the aircraft cuts back the thrust to idle and descends to the reference altitude h_{ref}, in this case 1000 ft. By this point the aircraft should be fully configured for a stabilized approach with a constant speed, attitude, and power setting. To meet the noise goal, the aircraft should just reach the final approach speed V_{APP}, in the case of the Boeing B747-200 studied in this paper, 150 kts at h_{ref}.

B. Problem of Spacing

Varying wind conditions, aircraft with different deceleration profiles, and inconsistent pilot behavior all contribute to the uncertainty in the TDDA approach trajectory. The combination of these three factors explains the uncertainty in the descent profile of an aircraft flying a TDDA which makes it particularly challenging for controllers to space incoming traffic. Hence, larger than normal spacings are applied as a safety buffer with negative consequences on runway capacity. Capacity reduction in turn has adverse effects on airport economies and for this reason airports are reluctant to introduce noise abatement procedures on a large scale. Thus, the large scale introduction of the TDDA requires an advanced version of the TDDA that does not compromise runway capacity.

Various solutions have been proposed to bridge this gap. In one such solution developed at the Massachusetts Institute of Technology (MIT) by Ren et al. [13], the factors driving aircraft trajectory variations were characterized using a wind model, an aircraft weight model, and a pilot response model which were then combined with an aircraft simulator to form an integrated Monte Carlo simulation tool. The Monte Carlo simulation tool was used to predict aircraft trajectories under various operational conditions, while a separation analysis methodology was developed to analyze the probable evolution of separation between random aircraft pairs. The purpose of the separation analysis was to recommend a desired spacing at an intermediate metering point for air traffic controllers to ensure separation during the approach *before* aircraft were cleared for a TDDA.

Alternatively, the separation task can be delegated to the pilot by providing the pilot with a sophisticated in-trail aircraft trajectory prediction algorithm combined with a flap scheduler algorithm [14,15]. Monte Carlo simulations indicate that this system could increase the runway throughput to 98% of the capacity of a conventional ILS approach [11]. Research has shown that safe separation is not jeopardized by this procedure and that workload is comparable to standard ILS approaches [14,16]. However, a drawback of the procedure is the so-called "slinky effect." The slinky effect can best be explained by an analogy with cars. When one car in a stream of traffic does not drive at a constant speed, cars trailing behind are constantly speeding up and slowing down to maintain safe separation with the preceding car. Because of the inherent time lag between when each driver adjusts speed, the cumulative effect of the decelerations and accelerations throughout the stream of traffic leads to severe spacing problems. This is known as the slinky effect. The same effect can be observed with a stream of incoming aircraft before a runway [17]. The underlying reason is that pilots concentrate solely on the approach behavior of the preceding aircraft without taking the behavior of the trailing aircraft into account. For example, in case the trajectory prediction algorithm foresees that the preceding aircraft is slowing down in such a way that minimum safe separation may be violated, the logic of the flap scheduler algorithm may set the flap selection speeds to their highest boundaries to decelerate the aircraft faster. However, the consequence of this new flap setting on the approach behavior of in-trail aircraft is not accounted for, potentially leading to an instability in the chain of approaching aircraft and leading to the slinky effect.

C. Time-Based Separation

An alternative to the self-separation TDDA procedure is presented in this paper. Rather than spacing aircraft based on trajectory prediction of the preceding aircraft, a solution is proposed in which aircraft are spaced by time. Incoming aircraft are provided by ATC with an RTA based on the aircraft configuration and the prevailing weather conditions. Pilots are required to adhere to the commanded RTA within given boundaries. By allowing each aircraft to navigate within predetermined time boundaries related to a minimum safe separation, pilots do not react to preceding or in-trail aircraft, thereby minimizing the likelihood of the slinky effect occurring further. It can then be hypothesized that runway capacity will not be compromised because of the reduction of the uncertainties in the descent profile, allowing tighter spacing and the minimization of the instabilities in the chain of arriving aircraft.

III. Wind Profile in the Terminal Maneuvering Area

To enable time-based separation, a deeper understanding of the uncertainties in the TDDA trajectory is required. A major source of uncertainty is the behavior of the wind in the TMA. Most of the TDDA takes place above the planetary boundary layer (PBL). The descent procedure takes the aircraft through the troposphere, which consists of the free atmosphere and the PBL. The behavior of the wind in the free atmosphere is governed by different dynamics than in the PBL. This has implications on the modeling of the wind profile along the approach trajectory. Because of this inherent indeterministic nature of the wind, this research introduces a stochastic model using zero-dynamic Kalman filtering to predict the behavior of the wind.

IV. Algorithm Design

Before elaborating on the details of the algorithm, the operational concept will be explained to gain a better understanding of the

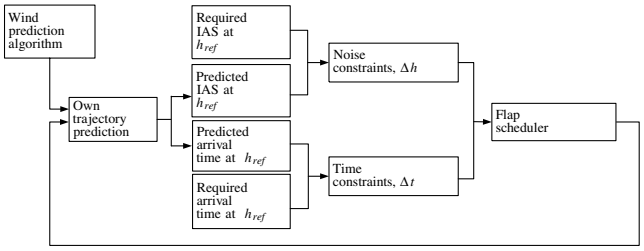

Fig. 2 The flap scheduler algorithm.

application of the algorithm in practice. Incoming aircraft are set up and spaced apart by ATC at a metering point roughly 25 nm from the runway at 7000 ft with a time slot and an RTA, which is based on the aircraft type and the prevailing wind conditions. By this time, the wind prediction algorithm, incorporated in the flap scheduler algorithm [14,15], has made a prediction of the wind profile along the approach trajectory. This wind profile serves as input for the own trajectory prediction module, which makes a time-to-fly estimate, which is used by the flap scheduler algorithm to determine the thrust-cut-back altitude and the flap schedule required to meet the noise target. The thrust-cut-back altitude, flap schedule, and deviation from the RTA are then integrated into a pilot support system that enables RTAs commanded by ATC to be met. Similarly, increased certainty that RTAs will be met allows ATC to space aircraft more tightly and as a result preserve runway capacity while meeting noise reduction targets.

A. Outline Flap Scheduler Algorithm

The flap scheduler algorithm, designed by in 't Veld [14] and De Prins and Schippers [15], was adopted for time-based separation and the wind predictor was incorporated into the routine. This paper treats the wind prediction algorithm in detail, while only an outline of the rest of the flap schedule algorithm will be given.

The basic structure of the algorithm is illustrated in Fig. 2. The wind predictor estimates the wind profile in the TMA and provides input for the own trajectory prediction module, which in turn is called by the flap scheduler algorithm to determine a thrust-cut-back altitude and flap schedule to meet the noise target. The algorithm loops through this iteration once every second.

The own trajectory prediction module of the flap scheduler algorithm predicts speed, distance, and time profiles of the aircraft along the approach trajectory. It is based on a simple aerodynamic model of the B747-200. The model is a point mass that only looks at the forces along the flight path and perpendicular to it. The resulting accelerations along the flight trajectory are integrated over time to yield speed, distance, and time profiles. The flap scheduler algorithm calls the own trajectory prediction module to determine a thrust-cut-back altitude and a flap schedule that will result in the aircraft decelerating to V_{APP} at h_{ref}. The thrust-cut-back altitude is the altitude at which the thrust should be set to idle so that V_{APP} can be reached at h_{ref} using the nominal flap schedule (Table 1). Once the thrust has been set to idle the algorithm corrects for deviations by adjusting the flap schedule so that the aircraft reaches V_{APP} at h_{ref}.

The flap scheduler algorithm by in 't Veld was augmented with the RTA optimization routine to improve the feasibility of time-based spacing. The time optimization is based on the commanded RTA. The RTA commanded by ATC is compared with the estimated time of arrival determined by the own trajectory prediction algorithm. The

Table 1 Upper bound, nominal, and lower bound flap speeds in knots, as used for the simulations, B747-200. The upper limits are determined by flap placard speeds, the lower limits by the minimum safe speeds at the flight mass used for the simulation

Flaps	5°	10°	20°	25°	30°
Upper bound (kts)	248	240	230	205	180
Nominal (kts)	215	200	190	165	158
Lower bound (kts)	205	190	165	158	151

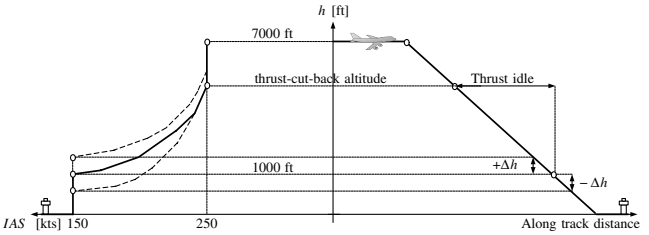

Fig. 3 The three-degree decelerating approach. For the nominal profile, the aircraft reaches V_{APP} at h_{ref}. If the aircraft decelerates too fast, the aircraft reaches V_{APP} too high, resulting in a positive Δh and a positive Δt. If the aircraft decelerates too slow, the aircraft overshoots h_{ref}, resulting in a negative Δh and a negative Δt.

deviation from the RTA is known as Δt, which can be either positive or negative. A positive Δt indicates that the aircraft is late and a negative Δt implies that the aircraft is early (see Fig. 3). The algorithm works in two modes. In the first mode the routine checks if Δt is within a 10 s boundary, and if this is true the routine optimizes solely for noise. It is also possible to bring Δt to zero by delaying or anticipating the selection of flaps indicated by the flap scheduler algorithm. However, if the time goals are violated the routine switches to the second mode and prioritizes the time optimization and drops the noise optimization goal. It sets the flap speeds to its upper boundaries if Δt is negative (i.e., aircraft is fast) to slow the aircraft, or to its lower boundaries if Δt is positive (i.e., aircraft is slow), until Δt is within the boundaries again.

B. AMDAR Wind Prediction Algorithm (AWPA)

The spatial and temporal variations of the wind affect the deceleration of the aircraft along the approach trajectory in the Earth-fixed reference frame. Accurate knowledge of the wind profile in the TMA is therefore required for an accurate own trajectory prediction and time-to-fly estimates. This in turn allows a thrust-cut-back altitude and flap schedule to be determined that will allow the noise and time goals to be met. The wind profile was modeled using a statistical model. The advantage of such a model is that it does not rely on the laws of physics that govern wind behavior, but instead uses past observations to construct a wind prediction.

The structure of the algorithm that drives the wind prediction model is shown in Fig. 4a. The wind prediction model is driven by historical automated meteorological data relay (AMDAR) data. AMDAR data consist of meteorological observations such as wind speed and direction as well as position coordinates. They are broadcast through the Aircraft Communications Addressing and Reporting System (ACARS) to in-trail aircraft which then store the historical data in a flight management system (FMS) database. The data are processed to make estimates of the current and future wind profile by making predictions based on the historical data. The algorithm is designed with a high-traffic scenario in mind but when the number of historical AMDAR observations available is scarce (e.g., between arrival and departure peaks), a wind profile can still be constructed using the available data, without making predictions, however.

The algorithm consists of three steps, as illustrated by Fig. 5. First, AMDAR data of preceding aircraft, each tagged with a corresponding time and altitude interval, is collected and stored in the FMS. Second, per altitude interval, the historical AMDAR data are filtered using a Kalman filter to remove measurement noise from the observations. The series of historical AMDAR data are then used to determine an autoregressive model of the time series. Third, the wind profile is constructed by connecting the predictions per altitude interval by linear interpolation.

1. *AMDAR Data*

One key input to the wind prediction algorithm is meteorological data in the TMA. With the transmission of AMDAR data to in-trail aircraft a wealth of meteorological information will become available for processing in the FMS. ACARS is the communication

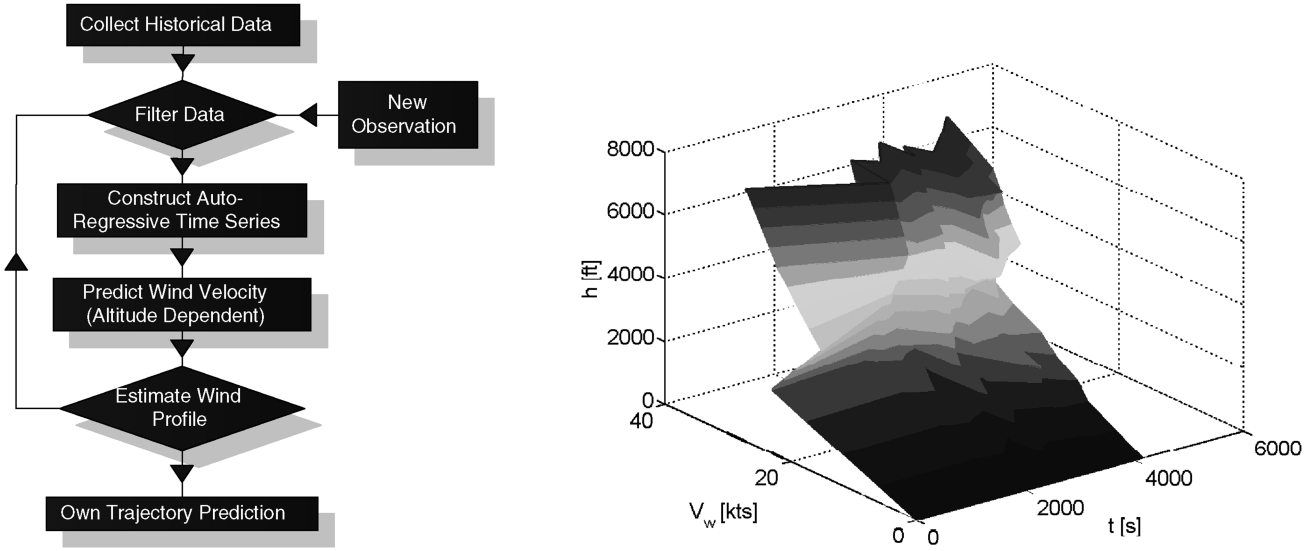

a) Structure of the wind prediction algorithm

b) Time-dependent wind profile at Chicago O'Hare on 7th of January 2005

Fig. 4 The wind prediction algorithm allows predictions to be made of the wind profile in the TMA.

system used by aircraft to broadcast AMDAR reports. The AMDAR reports consist of meteorological measurements made onboard the aircraft. The measurements are made by the pitot static head to determine static and total air pressure, an immersion thermometer probe to determine total air temperature, and an inertial reference platform to determine the aircraft normal, longitudinal, and lateral accelerations. These data are processed by the air data computer (ADC). It outputs pressure altitude derived from static pressure and static air temperature derived from total air temperature and Mach number. The ADC outputs position latitude and position longitude and computes the wind speed using true airspeed (TAS) corrected for Mach number and temperature. By resolving the vectors for ground speed and true airspeed the wind vector can be computed.

The spatial coverage of AMDAR data makes it suitable for the wind prediction algorithm as the observations are made along the TDDA trajectory. Temporal coverage of AMDAR data is highly variable due to evening peaks and early morning minima of commercial air traffic. However, the wind prediction algorithm is most suited for a high density traffic environment where aircraft spacing is critical to maintain high runway capacity.

The accuracy of AMDAR data depends on instrument measurement errors. Sources of error include calibration error, short-term random instrument error, calibration drift, and static source error. These errors are corrected as much as possible by the ADC. Typical uncertainty of AMDAR data is in the range between 2 and 3 m/s [18]. System cross-checks, gross error limits, and outlier rejection are various methods used by the onboard quality monitoring system to eliminate bad data. Note that these measurement and quality monitoring systems may differ per aircraft type, which subsequently may affect the accuracy of the AMDAR data.

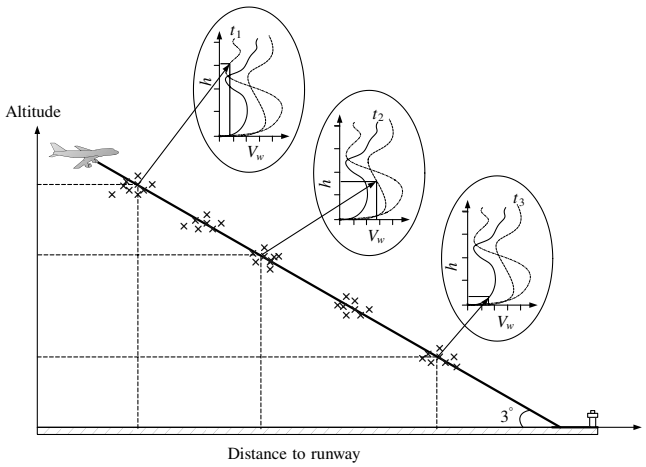

Fig. 5 Time-dependent wind profile prediction. Spatially distributed AMDAR observations are represented by crosses. Each set of AMDAR observations along the approach trajectory is associated with an altitude, a longitude, and a latitude.

2. *AMDAR Data Broadcasting*

An analysis of AMDAR broadcasts showed that AMDAR data are not broadcast at fixed altitude or time intervals. Although a more sophisticated wind prediction algorithm should work with AMDAR data broadcast at varying altitude and time intervals, the AWPA developed for this research requires that AMDAR data are broadcast at constant 500 ft altitude intervals. This choice of a constant altitude interval is preferred over a constant time interval broadcast because it can be assumed that the wind profile primarily depends on altitude and less on time due to the relatively fast update rate (±25–30 s). A consequence of broadcasting AMDAR data at constant time intervals would be that AMDAR data points are scattered not only in the horizontal but also in the vertical plane due to different deceleration rates along the TDDA trajectory. This scatter can be on the order of hundreds of feet, obtaining a less accurate interpolation of the wind profile. This effect is illustrated in Fig. 6. In Fig. 6a traces are shown for an aircraft that is broadcasting AMDAR data at constant time intervals, resulting in a scatter of data points along the vertical. In Fig. 6b traces are shown for the same aircraft broadcasting AMDAR data at constant altitude intervals, resulting in unevenly spaced time intervals.

Variations of the wind speed along the vertical plane adjacent to the Earth's surface are more significant than in the horizontal plane parallel to the Earth's surface. Assuming the vertical wind speed to be negligible, AMDAR observations are grouped into altitude intervals to make predictions of wind speed variations in the vertical plane.

By broadcasting data at constant altitude intervals, a series of AMDAR data are collected that are unevenly spaced in time and unevenly spaced in the horizontal plane. Assuming that this uneven spatial and temporal spacing in the horizontal plane has negligible effects on the accuracy of the wind speed observations, a series of AMDAR observations are available for processing by the flight management computer.

3. *Kalman Data Filtering*

Once the AMDAR data have been broadcast, stored in the FMS, and grouped in altitude intervals, the data are filtered using a Kalman

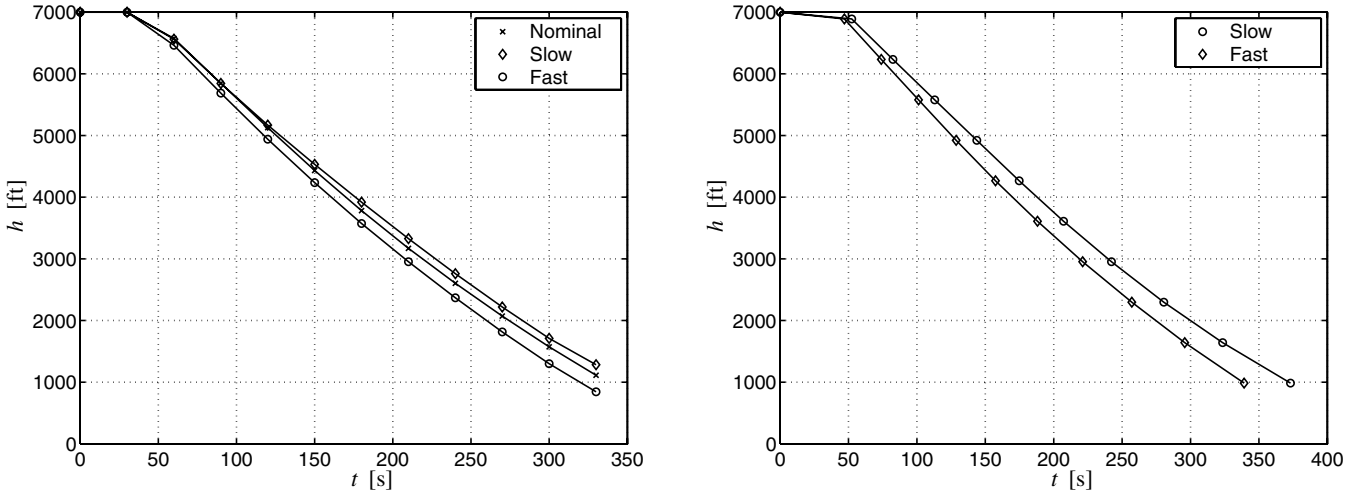

a) Constant time interval **b) Constant altitude interval**

Fig. 6 AMDAR broadcasting strategies. By broadcasting AMDAR data at fixed altitude intervals, the data are unevenly spaced in time. Likewise, by broadcasting AMDAR data at fixed time intervals, the data are scattered in the vertical plane. Note that a fast descent is caused by tardy flap extension, whereas a slow descent originates from aggressive flap extension with respect to the nominal flap extension schedule.

filter with no model dynamics. The Kalman state equation and measurement equation are given by, respectively,

$$v_{t+1} = \phi_t v_t + w_t \qquad z_t = H_t v_t + u_t \tag{1}$$

In Eq. (1) v_{t+1} is the state estimate of the wind speed at time $t+1$, ϕ_t is the transition matrix, and w_t is the process noise. The second equation is the observation where z_t is the measured wind speed at time t, H_t is the measurement matrix, and u_t is the measurement noise resulting from onboard instrument measurement errors. The absence of model dynamics reduces the Kalman filter equations to a simple set of equations with the transition matrix $\phi_t = 1$ and the observation matrix $H_t = 1$. In the first step of the Kalman filter the error covariance P_t, with the process noise covariance Q_t, is projected ahead. The size of the Kalman gain K_t depends on the projection ahead of the error covariance P_t, together with the measurement noise covariance R_t. The size of the Kalman gain then determines how much weight is given to the wind speed measurement z_t, from which follows an update of the state estimate of the wind speed v_t. In the last step of the Kalman filter the error covariance is updated. This iteration is repeated with a constant time step of 60 s.

$$\begin{aligned} P_{t+1} &= P_t + Q_t \qquad K_t = P_t(P_t + R_t)^{-1} \\ v_t &= v_t + K_t(z_t - v_t) \qquad P_t = (I - K_t)P_t \end{aligned} \tag{2}$$

The value of the process noise covariance Q_t and the measurement noise covariance R_t was determined empirically by a Monte Carlo simulation. By taking the transition matrix $\phi_t = 1$ and the observation matrix $H_t = 1$, the performance of the Kalman filter is determined entirely by the selection of the values for Q_t and R_t. The prediction estimate is therefore based on a combination of the measured wind speed z_t, the process noise covariance Q_t, and the measurement noise covariance R_t.

4. *Autoregressive Least Squares Wind Prediction*

By filtering the data with a Kalman filter, measurement noise was reduced. The filtered series of AMDAR observations represent the historical evolution of the wind speed up to the present time. The next step in the AWPA involves the prediction of the wind speed in the future by making an autoregressive (AR) model of the filtered time series. The model coefficients can be used to make predictions of the wind speed along the TDDA trajectory. An efficient method to estimate the coefficients of the AR model is by least squares [19]. Note that the filtered time series are not evenly spaced, but the deviations are in the order of seconds. The assumption is made that the change in wind speed in that interval is negligible, and therefore an evenly spaced time series is assumed.

An m-variate AR model of order p can be described by

$$v_t = w + \sum_{l=1}^{p} A_l v_{t-l} + \varepsilon_t, \qquad \varepsilon_t = \text{noise}(C) \tag{3}$$

It is a model for a stationary time series of state vector v_t that has been observed at equally spaced time instants t. The matrix A is made up of the coefficients of an AR model, and the vector $\varepsilon_t = \text{noise}(C)$ is an uncorrelated random vector with mean zero and covariance matrix C. The vector w is an intercept term which allows for a nonzero mean of the time series.

For the selection of the order p of an AR(p) model and for the estimation of the parameters w, A, and C, a stepwise least squares algorithm is implemented. In the stepwise least squares algorithm, the order selection criteria are evaluated for models of order $p_{\min}, \ldots, p_{\max}$ by stepwise downdating a regularized QR factorization for a model of order $p_{\max}$. From the QR factorization for a model of order $p_{\max}$, approximate least squares estimates of the parameters w, A, and C are computed for the model of the order p_{opt} that optimizes the order selection criterion, in this case Schwarz's Bayesian criterion (SBC). Order selection criteria, such as Schwarz's Bayesian criterion, represented by Eq. (4), are usually functions of the logarithm of the determinant:

$$\text{SBC}\,(p) = \frac{l_p}{m} - \left(1 - \frac{n_p}{N}\right)\log N \tag{4}$$

The estimates of the coefficients of the AR model allow a prediction to be made of the wind speed t steps ahead. By recursively multiplying the coefficients of the nth order AR model with the last n wind speed measurements, a prediction can be made of the wind speed t steps ahead. In Eq. (5), ϕ_n are the coefficients of an nth order AR model:

$$\hat{v}_t = \phi_1 v_{t-1} + \phi_2 v_{t-2} + \cdots + \phi_n v_{t-n} \tag{5}$$

5. *Wind Profile Construction and Performance*

The output of the algorithm is a set of predictions per 500 ft altitude interval which represent the evolution of the wind speed along the time axis, starting from the present time of the aircraft until the time t minutes ahead at the end of the TDDA procedure. For each prediction step, the wind profile is constructed by connecting the predictions per altitude interval by linear interpolation. Also, the wind profile between prediction steps is determined by linear interpolation.

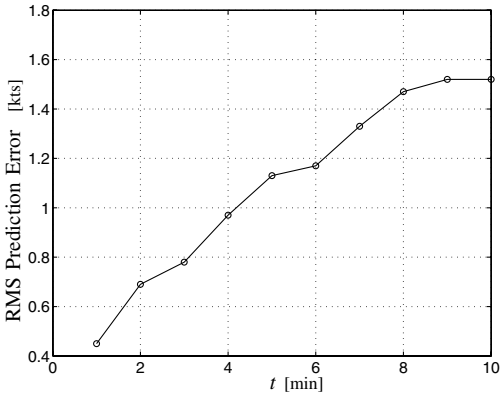

Fig. 7 Wind prediction performance.

The performance of the wind profile prediction algorithm was tested with AMDAR observations at Chicago O'Hare collected over the period of a week in the first week of January 2005. The AMDAR observations were interpolated along the altitude axis as well as along the time axis. The performance of the wind prediction algorithm was tested for time steps between 1 and 10 steps ahead. As can be seen in Fig. 7, performance of the algorithm decreases with increasing prediction time, but was judged to be adequate for the flap scheduler algorithm.

V. Monte Carlo Simulation

To validate the AWPA in combination with the flap schedule algorithm, a Monte Carlo simulation was done. By collecting AMDAR data from in-flight measurements at Chicago O'Hare airport, a large sample of actual time-dependent wind profiles as shown in Fig. 4b could be reconstructed to be used for the Monte Carlo simulations. Headwinds, crosswinds, and tailwinds were reconstructed by taking three different wind directions of 360, 180, and 315°, respectively. Each wind condition was given a gradual rotation up to a maximum of 30° at the Earth's surface. The performance of the flap scheduler algorithm was compared for two different wind profile prediction algorithms, namely, the AMDAR wind profile prediction algorithm and the logarithmic wind profile algorithm [15].

A. Results

In Figs. 8a and 8b the results of the Monte Carlo simulation are shown for the comparison of the AMDAR algorithm with respect to the log algorithm. The error bars show that the AMDAR algorithm is able to meet the noise goals more accurately than the log algorithm. Clearly, the performance of the log algorithm is worse than the AMDAR algorithm due to poor wind profile prediction, illustrated in Fig. 8c. The result of a poor prediction is an under- or overestimate of the thrust-cut-back altitude, leaving little or no control space for the flap scheduler to compensate for earlier errors. As a result, the aircraft reaches V_{APP} far before h_{ref}. For the tailwind condition the log algorithm tends to underestimate the wind speed which results in V_{APP} being reached below h_{ref}. For a headwind and the crosswind condition, the algorithm tends to overestimate the wind speed which results in the aircraft decelerating too fast and reaching V_{APP} too early.

B. Control Space Analysis

To determine the feasibility of a TDDA while spacing aircraft by time, an insight is required into the control space limits of the flap scheduler algorithm. The control space limits define the maximum and minimum feasible deceleration rates for a given aircraft configuration and wind condition in which noise and time goals can still be met [20]. The limits of the control space depend on a number of factors such as aircraft type and weight, the prevailing wind conditions, and the flap placard speeds. In this research the aircraft type and weight were fixed, but the wind conditions were varied.

The control space limits were determined for four wind conditions: a headwind, a crosswind, a tailwind, and zero wind. A representative mix in terms of profile shape and wind speed was selected from the wind profiles used for the Monte Carlo simulation. The tailwind condition was included for sake of completeness and to gain insight in the performance of the AWPA, but was omitted during the piloted experiment because approaching and landing with a tailwind are not considered normal operational practice.

Along with the nominal path, which yields the largest amount of control space authority, there is a path of early deceleration and a path of late deceleration. The path of late deceleration is the fastest path and sets all the flap speeds to their lower bounds. The path of early deceleration is the slowest path and sets all the flap speeds to their upper bounds. The difference between the early path and the late path of deceleration defines the control space limits. Figure 9 illustrates this for the zero-wind case. The control space limits for different wind conditions with different directions are given in Table 2. Clearly, the tailwind condition and the zero-wind condition have the smallest and the largest control space, respectively.

The results of the control space analysis indicate that under favorable circumstances (i.e., zero-wind condition), the control space for noise and time (30 s) is greatest, while for the tailwind condition the control space is smallest (8 s). Based on these results it would therefore make sense to determine nominal RTAs for both ATC and airlines so that sufficient control space is left to execute the TDDA while meeting time targets. By commanding RTAs that are based on maximum control space to meet noise and time goals, uncertainty in pilot behavior and wind can be accounted for.

VI. Piloted Experiment

The Monte Carlo simulations validated the AMDAR wind prediction algorithm and determined the control space limits in terms time. To test the effectiveness and assess the operational uncertainties of time-based spacing under actual wind conditions, a piloted experiment was conducted in a six-degree-of-freedom research flight simulator. The goal of this experiment was to determine the effect of different scenarios on performance in terms of noise, time, and workload.

A. Pilot Support Interface Design

A pilot support interface, known as the decelerating approach support system (DASS), was developed so that the flap schedule, the thrust-cut-back information, and time-to-fly estimates determined by the flap scheduler algorithm could be presented to the pilot in a meaningful way. In this experiment, the designed display has been compared to a standard cockpit interface with a previously developed cueing system [20] which serves as a baseline condition.

1. DASS Display

The DASS display was designed in such a way that the display would support the pilot in his/her task of accurately flying the TDDA with only flaps to control the deceleration of the aircraft while meeting noise and time goals. Equally so, the display was designed in such a way that it did not differ significantly from current display formats to avoid modification problems with existing displays and to avoid problems with pilot acceptance [14]. The primary flight display (PFD), shown in Fig. 10a, is augmented with a thrust cue and a flap cue. The thrust cue, represented by the letter "T" on the altitude tape of the PFD, helps the pilot to determine the altitude at which the thrust can be set to idle for the prevailing wind conditions using a nominal flap schedule. The flap cue is displayed on the speed tape, represented by the letter "F," and informs the pilot when to select the next flap stage.

To aid the pilot with meeting the commanded RTA, the navigation display (ND) shown in Fig. 10b is augmented with a time performance indicator, represented by ΔT. Beneath the ΔT symbol is the estimated deviation in seconds from the RTA. A negative ΔT means that the aircraft is fast and a positive ΔT means that the aircraft is slow. To warn the pilot that the time separation margins are being

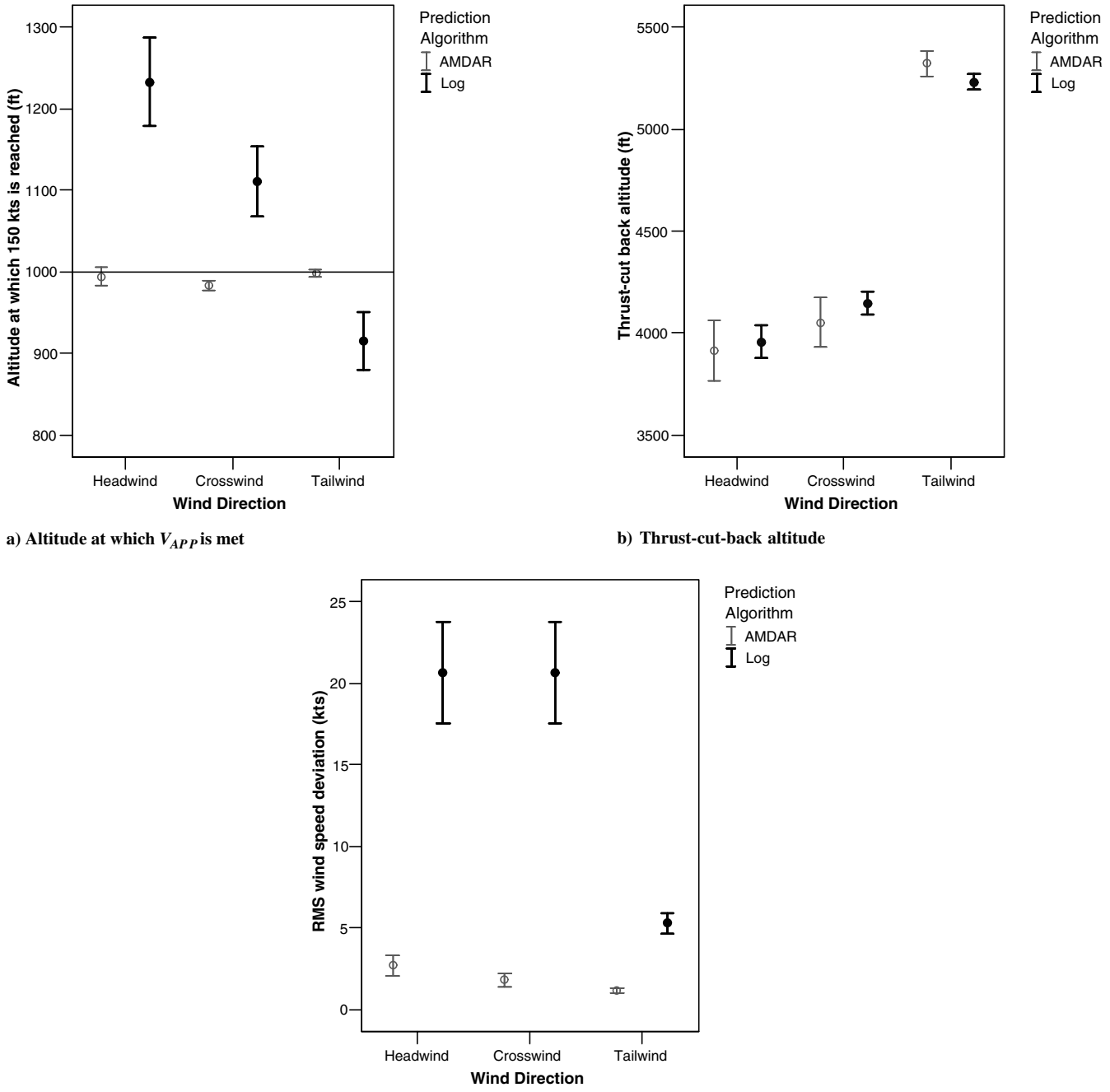

a) Altitude at which V_{APP} is met

b) Thrust-cut-back altitude

c) RMS of the wind speed prediction error

Fig. 8 The Monte Carlo simulations show that the AMDAR wind profile prediction algorithm performance is better than for the log algorithm (solid filled circles). The AMDAR algorithm can "see" further down the trajectory and therefore the flap scheduler algorithm can determine a more accurate thrust-cut-back altitude and flap schedule.

exceeded, an amber annunciator lights up displaying either "FAST" or "SLOW," respectively, for a negative and a positive ΔT. In addition, a second clock, positioned below the clock displaying the actual time in the upper right-hand corner of the ND, displays the RTA.

2. Design Baseline Condition

The baseline condition consisted of a cueing system developed previously by Ho [20] that does not require additional aircraft automation to help pilots manage the deceleration of the aircraft and achieve target conditions in a changing environment. The cueing system, consisting of "gates" (i.e., altitude/speed checkpoints) and a recommended flap schedule, was shown to reduce target error to within 5 kts and provide comparable performance to that of more automated systems without increasing pilot workload.

For this research, the pilot cueing system was augmented with a greater domain of wind conditions and additional time checkpoints. Three different wind conditions—zero wind, 30 kts headwind, and a 60 kts headwind—with each their own system of gates was represented on the cueing system. The wind profiles were based on standard logarithmic profiles. The time checkpoints serve as a reference with respect to the commanded RTA. By noting the wind at 7000 ft and the wind on the ground the pilot could determine a series of gates appropriate for the approach trajectory by interpolating between altitude, speed, and time checkpoints.

B. Method

1. Independent Variables

First, two displays were defined. The first display, for the baseline condition, was a conventional PFD/ND display layout. The second

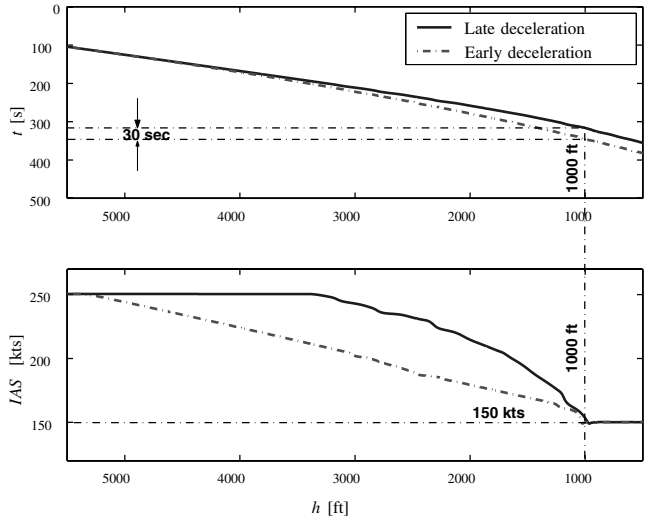

Fig. 9 The control space authority for the flap scheduler algorithm for the no wind condition. Noise targets can be met for arrival times deviating by 30 s.

display, for the DASS condition, had a PFD and ND augmented with information derived from the flap scheduler algorithm.

Second, four different wind conditions were defined based on an analysis of the wind profiles used for the Monte Carlo simulation.

2. *Experiment Design*

The experiment matrix forms a 4 by 2 factorial design (see Table 3). Two display conditions multiplied by four wind conditions give eight conditions for each pilot. Ten professional pilots flew two blocks of eight conditions, preceded by two blocks of six training runs to familiarize the pilots with the procedure and the wind classes.

3. *Apparatus*

The experiment was conducted in the advanced six degrees-of-freedom motion-based research simulator of Delft University of Technology SIMONA. The PFD, the ND, and the mode control panel (MCP) of the B747-400 were projected on two 15 in. LCD screens. An outside visual was shown of a landscape with a fictitious airport.

4. *Aircraft*

The aircraft model was a nonlinear six-degrees-of-freedom model of the Boeing 747-200. It did not have a landing gear model. The aircraft was manually flown with the yaw damper on.

5. *Wind Conditions*

Four wind conditions were simulated including a zero-wind condition; see Fig. 11. Although a tailwind condition was included during the Monte Carlo simulations to investigate the performance of the AWPA, such a condition was omitted during the piloted experiment due to the operational improbability of flying an approach to landing with a tailwind. What sets the wind profiles apart from each other besides wind speed and direction is the number of speed inversions with respect to altitude. Class 0 wind is a zero-wind condition. Class 1 wind is a standard logarithmic profile with no speed inversions. Class 2 is a wind profile with one speed inversion where the wind speed tends to increase during the descent and then starts to decrease again. The class 3 wind represents a wind profile with two or more speed inversions. The wind speeds and directions for these four wind classes are given in Table 4. Turbulence was superimposed over the wind model [16].

6. *Procedure*

The task was to fly a TDDA while meeting noise and time goals. The aircraft started at an initial altitude of 7000 ft 25 nm out from the runway threshold at an indicated airspeed of 250 kts. At 22 nm from the threshold the aircraft captured the ILS and started its descent along a 3° glide slope. It continued its descent beyond the reference point h_{ref} up to 800 ft after which the simulator was stopped. The aircraft started with the autopilot and the autothrottle engaged with flaps 1° extended. As soon as the simulation started, the pilot would disengage the autopilot and the autothrottle.

7. *Dependent Variables*

Two types of dependent variables were collected during the experiment: 1) *objective* measurements from the aircraft parameters and the pilot inputs and 2) *subjective* measurements obtained from a pilot questionnaire as well as the NASA task load index (TLX) sheet after each run to assess pilot workload [21]. The objective measurements included pilot control actions and operational performance parameters with respect to noise and time goals.

8. *Hypotheses*

It was hypothesized that by using the DASS both the noise and the time goals would be met, regardless of the wind condition. It was expected that the pilot would concentrate on meeting the time goal (i.e., bringing Δt to zero) by adjusting the moment of flap selection while the algorithm determines the optimum flap schedule required for meeting the noise goal. For the baseline condition, however, it was hypothesized that noise and time goals would be met for wind classes 0 and 1 but not for wind classes 2 and 3. The reasoning for this was that the reference gates on the cue card would coincide closely for wind classes 0 and 1 and therefore would require little interpolation. Wind classes 2 and 3, however, were not common logarithmic profiles and therefore would require more pilot effort and cue card interpolation in order to meet the noise and time goals. It was hypothesized that the workload would be lowest for the DASS condition. Equally so, it was hypothesized that for the baseline condition the workload of the pilot would increase as the wind

Table 2 The control space limits for various wind conditions. The minima and maxima for the thrust-cut-back (TCB) altitude and arrival times are given

	Max. TCB altitude, ft	Min. TCB altitude, ft	Max. TDDA time, s	Min. TDDA time, s	Control space, s
Zero wind	5400	3400	346	316	30
Headwind	4100	2800	384	360	24
Crosswind	3500	2600	373	357	16
Tailwind	6200	5000	308	300	8

Table 3 Experiment matrix. The baseline condition is a standard display with an ND and a PFD. The DASS display is augmented with a thrust cue, a flap cue, and a time performance indicator. The wind conditions range from a class 0 to a class 3 wind condition, each with their own RTA

Wind/display	Class 0 zero wind	Class 1 headwind	Class 2 crosswind	Class 3 headwind
Baseline	⋆	⋆	⋆	⋆
DASS	⋆	⋆	⋆	⋆

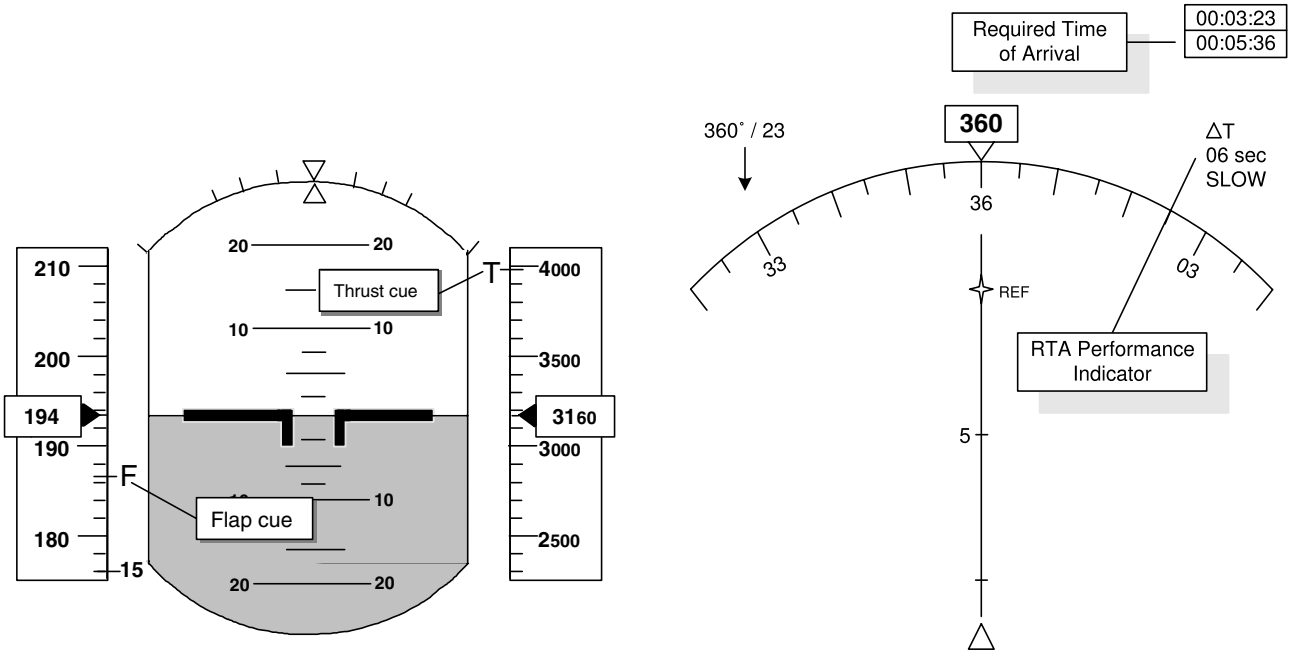

a) The primary flight display **b) The navigation display**

Fig. 10 The DASS pilot support interface consists of an augmented PFD and ND. The PFD is augmented with a flap cue and a thrust cue. The ND is augmented with a time performance indicator and an RTA indicator.

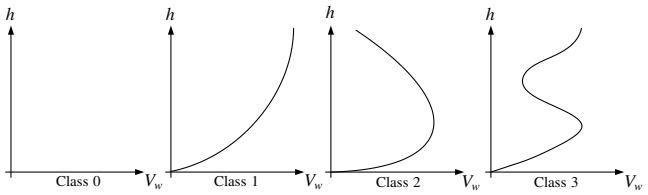

Fig. 11 Wind profile classification. The class number increases with the number of speed inversions. Class 0 is a zero-wind condition, class 1 represents a logarithmic profile, class 2 has one speed inversion, and class 3 has two speed inversions.

classification increases (i.e., an increase in the number of speed inversions in the wind profiles).

VII. Results and Discussion

A. TDDA Operational Performance

The two main factors that determine the operational performance of the TDDA are the altitude at which V_{APP} is reached (noise goal) and the deviation from the RTA (time goal).

1. Noise Goal

Figure 12a, which gives the means and the 95% confidence intervals for the altitude at which V_{APP} is reached, shows that for the DASS condition the performance is constant across the entire range of wind conditions, while performance of the baseline condition depends largely on the wind class. This observation is confirmed by an analysis of variance (ANOVA) which shows that the effect of the optimization on the TDDA performance is significant ($F_{1,9} = 7.859$, $p = 0.021$). The effect of optimization for both conditions if only wind classes 1, 2, and 3 are considered is highly significant ($F_{1,9} = 11.149$, $p = 0.009$). Clearly, for the zero-wind condition, the gates on the cue card correspond exactly to the nominal profile, aiding the pilot in the selection of a thrust-cut-back altitude and flaps without the need for interpolation. For wind classes 1, 2, and 3, however, the pilot is required to interpolate between gates on the cue card to meet noise and time goals. For wind class 1, which resembles a logarithmic profile, pilot performance is comparable to the DASS condition but the standard deviation with respect to the altitude at which V_{APP} is reached is greater. For wind classes 2 and 3, pilot performance is worse than for the DASS condition and this is primarily the result of poor thrust-cut-back altitude selection, shown in Fig. 12c. Accurate thrust-cut-back altitude selection is a key parameter for accurate TDDA performance. For wind class 2, pilots underestimate the wind profile and set the throttle to idle too early. The result is that the aircraft decelerates too fast and V_{APP} is reached too early.

Table 4 The wind speeds, directions, and headwind components at 7000 ft for each wind class

	Wind speed, kts	Wind direction (°)	Headwind component, kts
Class 0	0	0	0
Class 1	49	360	49
Class 2	27	315	19
Class 3	34	360	34

The importance of the wind prediction algorithm for the thrust-cut-back altitude selection immediately becomes clear. The wind prediction algorithm can "see" further down the trajectory and therefore select an appropriate thrust-cut-back altitude. An accurate thrust-cut-back altitude selection positions the aircraft in the middle of the control space, allowing for the greatest control space authority. This effect can clearly be seen for wind class 2. For the DASS condition, the thrust-cut-back altitude is centered around 3400 ft because the wind prediction algorithm can predict the increase in wind speed at 4000 ft. Pilots are unable to do this for the baseline condition and this is clearly shown in the selection of a thrust-cut-back altitude at 4000 ft, resulting in poor TDDA performance.

2. Time Goal

Figure 12b shows that the deviation from the commanded RTA for the DASS condition is centered around zero for wind classes 0 and 3 while it is very close to zero for wind classes 1 and 2. For the baseline condition, however, the deviations from the RTA are much larger and primarily the result of poor thrust-cut-back altitude selection. For class 0, for example, the selected thrust-cut-back altitude corresponds to the gates on the cue card and hence the deviation from the RTA is small. For wind class 2, however, a poor estimation of the thrust-cut-back altitude leads to a fast deceleration to V_{APP} and

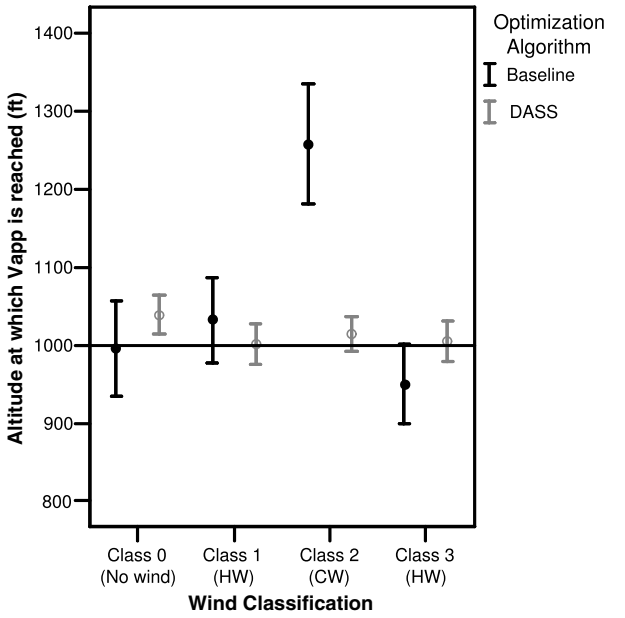

a) The means and the 95% confidence intervals for the altitude at which V_{APP} is reached

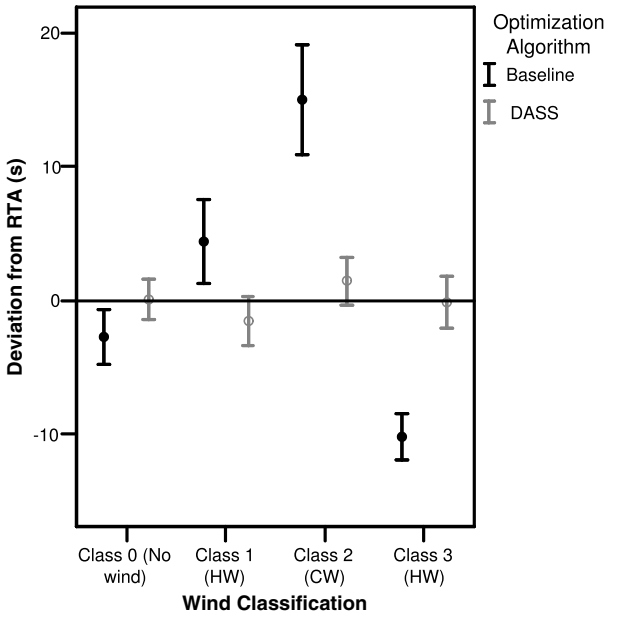

b) The means and the 95% confidence intervals for the deviation from the RTA at h_{ref}

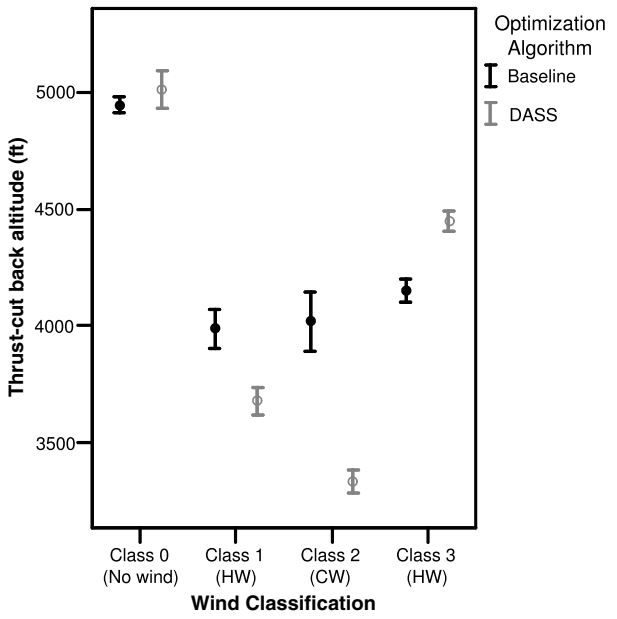

c) The means and the 95% confidence intervals for the thrust-cut-back altitude

Fig. 12 The TDDA operational performance is measured by the altitude at which V_{APP} is reached and the deviation from the RTA. The performance for the DASS condition is consistent for all four wind classes while the baseline condition shows inferior performance, especially for wind classes 2 and 3.

therefore a late arrival at h_{ref}. The DASS condition clearly reduces the likelihood of exceeding the 10 s separation margin, and this is reflected in Fig. 13a. By meeting the RTA, the aircraft operates within the control space limits and this allows noise and time goals to be met. ANOVA validates the observed performance and showed indication that the effect of the optimization on meeting the RTA is highly significant ($F_{1,9} = 61.230$, $p < 0.001$).

B. Pilot Control Activity

1. *Flap Activity*

The flap activity, shown in Fig. 13b, indicates that the majority of runs were with five flap selections. Nominally the aircraft should be configured with flaps 30 deg at the end of the run, resulting in five flap selections. In a number of cases, however, fewer flaps were selected. This was mainly due to the fact that in some runs the pilot selected the thrust-cut-back altitude too early and therefore tried to compensate by selecting their flaps at their lower boundaries which meant that in some cases the pilot did not extend all the remaining flaps before passing h_{ref}.

2. *Pilot Adaptation*

Once the throttle has been set to idle, pilots only have flaps to control their deceleration. For the DASS condition, pilots follow the flap cues closely unless they are trying to compensate for deviations from the commanded RTA, as shown in Fig. 14b. Pilots delay or anticipate flap selection to bring Δt to zero. Because the algorithm determines a thrust-cut-back altitude that gives the greatest control space authority, pilots can anticipate or delay the flap selection to

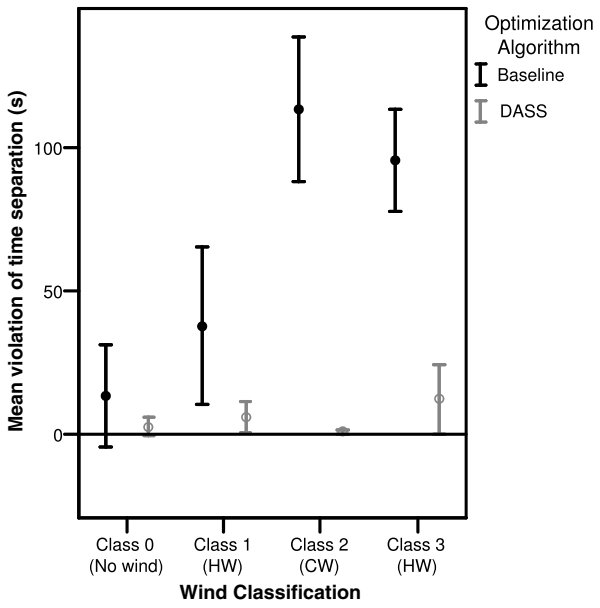

a) The means and the 95% confidence intervals for the deviations from the 10 second separation limit for the whole trajectory

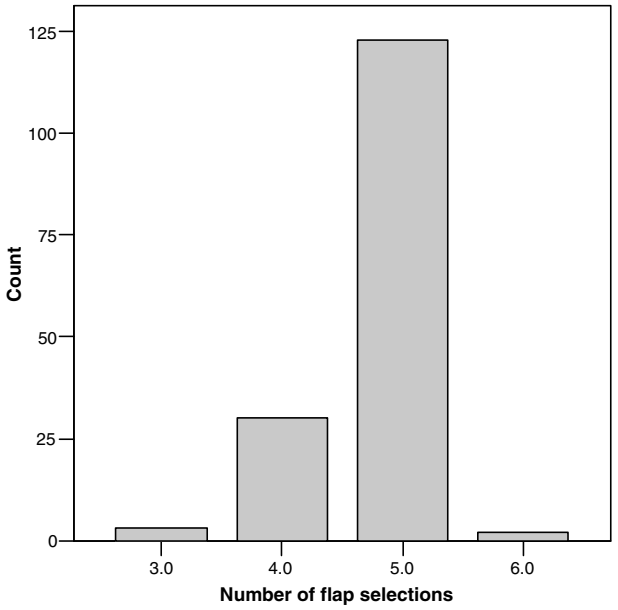

b) Number of flap selections during the decelerating approach

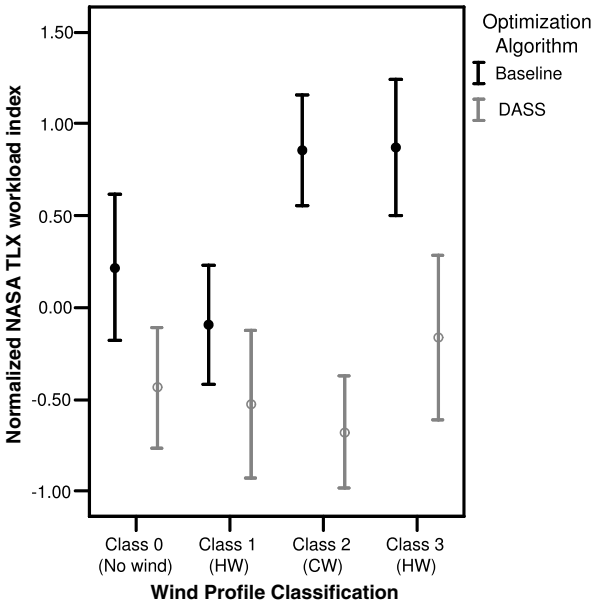

c) The means and the 95% confidence intervals for the normalized TLX ratings

Fig. 13 Pilot control activity in terms of flap and throttle selection. Violation of the separation margins is much higher for the baseline condition because the pilot has no reference to determine the deviation from the commanded RTA other than the gates on the cue card.

meet both noise and time goals. For the baseline condition, however, pilots only have the cue card as a reference. If the thrust-cut-back altitude is estimated poorly, resulting in the aircraft operating on the border of or outside the control space, pilots tend to adapt the flap selection based on their estimated progress, as shown in Fig. 14a. Especially for wind class 2, where the thrust-cut-back altitude was selected too early, pilots tend to delay the selection of flaps to minimize the deceleration of the aircraft in an attempt to meet V_{APP} at h_{ref}.

C. Pilot Workload

The results for the normalized NASA TLX ratings are shown in Fig. 13c. The workload for the DASS condition is consistently less than for the baseline condition. This is confirmed by ANOVA. The effect of the optimization on the workload is highly significant ($F_{1,9} = 27.043,\ p = 0.001$), as is the effect of the wind condition ($F_{3,27} = 7.259,\ p = 0.001$). The effect is less for classes 0 and 1, most likely because the wind conditions are relatively simple compared to classes 1 and 2. As a result, pilots are able to draw more on their pilot experience and intuition and therefore the workload is less. Wind classes 2 and 3, however, are more difficult than wind classes 0 and 1, resulting in a greater workload. Because of fast changing wind conditions pilots need to concentrate more on the control task in addition to determining the correct parameters for accurate TDDA performance.

VIII. Conclusions

The algorithms and pilot support interface presented in this paper have been designed to enable TDDAs with time-based separation by reducing the uncertainties in the approach trajectory during the TDDA (pilot behavior, aircraft aerodynamic performance, and wind conditions). A wind prediction algorithm based on historical

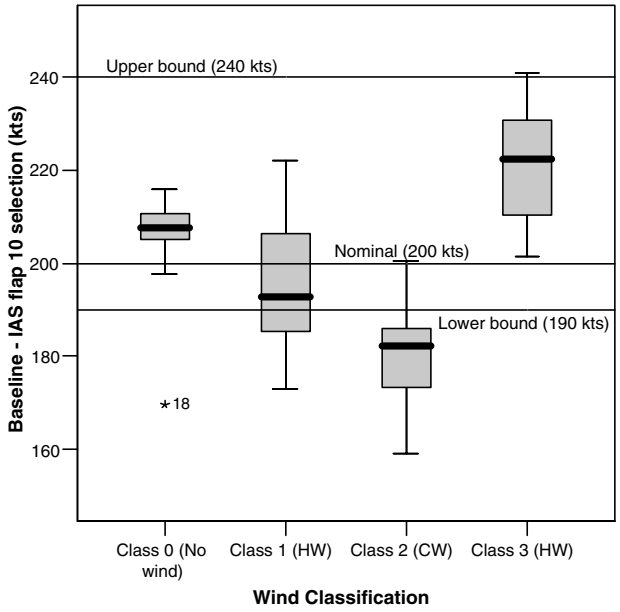

a) Boxplots representing the median and the interquartile range for flap 10° selection for the base line condition

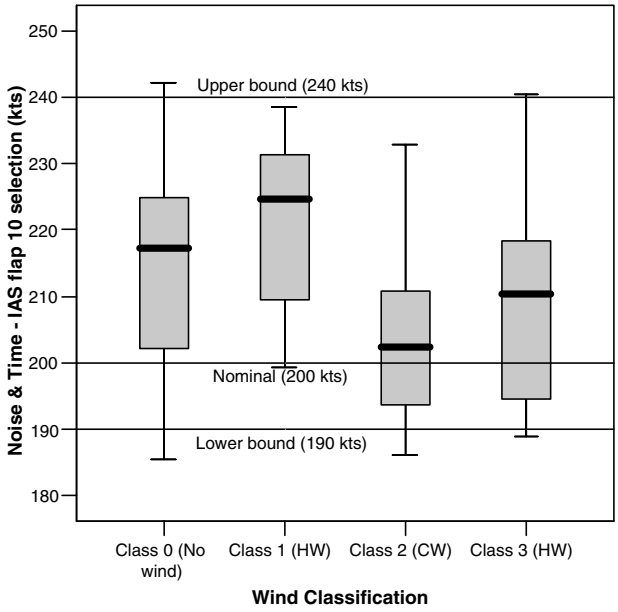

b) Boxplots representing the median and the interquartile range for flap10° selection for the DASS condition

Fig. 14 Pilots adapt their behavior to the estimated TDDA progress. For the baseline condition pilots seek the extremes of and even go beyond the flap boundaries, as for wind class 2, to slow the deceleration of the aircraft to meet noise and time goals. For the DASS condition pilots delay or anticipate flap selection to minimize the deviation from the commanded RTA.

AMDAR data from preceding aircraft in the TMA allows accurate estimates and predictions to be made of the wind profile. Improved wind profile prediction enables more accurate speed, distance, and time profiles to be made for the TDDA trajectory. As a result, an accurate flap schedule and thrust-cut-back altitude can be determined. By presenting this information to the pilot in a meaningful way through a pilot support interface, the pilot is able to meet both noise and time goals without increased workload, as compared with the baseline condition.

The piloted experiment indicated that noise and time goals could be met with the help of the pilot support interface, regardless of the wind condition. For wind classes 0 and 1, the least complex wind profiles, noise, and time goal performance were acceptable without the aid of automation. The increase in workload with respect to the automated condition was not significantly higher. For more complex wind conditions, however, such as wind classes 2 and 3, workload was significantly higher and pilots were unable to meet noise and time goals without the aid of automation. The ability of the wind prediction algorithm to "see" further down the trajectory allows the selection of an accurate thrust-cut-back altitude which gives the aircraft the greatest control authority. In this way the pilot can control the deceleration of the aircraft within the control space limits by selecting a path of fast or slow deceleration, while the algorithm takes care of meeting the noise goals. By relieving the pilot from the responsibility of meeting the noise target by automating the flap selection, the problem of meeting both noise and time goals is reduced to a first order problem which the pilot can solve.

IX. Recommendations

Monte Carlo simulations and the piloted experiment showed the potential of the wind prediction algorithm for flying a TDDA. It would be interesting to validate the algorithm in an actual flight test. Also, it would be worth looking into expanding the flap scheduler algorithm to a more sophisticated algorithm that determines a flap schedule and thrust-cut-back altitude that incorporates both noise and time targets, relieving the pilot from any extra workload. Future research should include simulations of a representative fleet mix to determine the impact on runway capacity. Finally the process of determining the RTA, spacing the aircraft by assigning these RTA to the aircraft, and the role of ATC in this scenario should be subject to further investigation.

References

[1] Clarke, J. P., and Hansman, R. J., "A System Analysis Methodology for Developing Single Event Noise Abatement Procedures," Ph.D. Dissertation, Massachusetts Institute of Technology, Department of Aeronautics and Astronautics, 1997.

[2] Wubben, F. J. M., and Busink, J. J., "Environmental Benefits of Continuous Descent Approaches at Schiphol Airport Compared with Conventional Approach Procedures," National Aerospace Laboratory, TR NLR-TP-2000-275, Amsterdam, The Netherlands, 2000.

[3] Erkelens, L. J. J., "Research into New Noise Abatement Procedures for the 21st Century," AIAA Paper 2000-4474, 2000.

[4] Koeslag, M. F., "Advanced Continuous Descent Approaches," Delft University of Technology & National Aerospace Laboratory NLR, TR NLR-TR-2001-359, Faculty of Aerospace Engineering, 2001.

[5] Anon., "Sourdine D3: Establishment of Noise Abatement Solutions," Sourdine Technical Report D3, Amsterdam, The Netherlands, 2000.

[6] Anon., "Sourdine D5: Final Report," Sourdine Technical Report D5, Amsterdam, The Netherlands, 2000.

[7] Tan Ho, N., and Clarke, J. P., "Mitigating Operational Aircraft Noise Impact by Leveraging on Automation Capability," AIAA Paper 2001-5239, 2001.

[8] Gershzohn, G., Wat, J., Dwyer, J. P., Elmer, K., Clarke, J. P., and Tan Ho, N., "Advanced Noise Abatement Procedures: An Experimental Study of Flight Operational Acceptability," *AIAA's Aircraft Technology, Integration, and Operations (ATIO) Technical*, AIAA, Reston, VA, 2002, pp. 1–9; also AIAA Paper 2002-5867.

[9] Elmer, K., Wat, J., Gershzohn, G., Shivashankara, B., Clarke, J. P., Tan Ho, N., Tobias, L., and Lambert, D., "A Study of Noise Abatement Procedures Using Ames B747-400 Flight Simulator," *8th AIAA/CEAS Aeroacoustics Conference & Exhibit*, AIAA, Reston, VA, 2002, pp. 1–10; also AIAA Paper 2002-2540.

[10] Elmer, K., Wat, J., Shivashankara, B., McGregor, D., and Lambert, D., "A Continuous Descent Approach Study using Ames B747-400 Flight Simulator," *AIAA's Aircraft Technology, Integration, and Operations (ATIO) Technical*, AIAA, Reston, VA, 2002, pp. 1–9; also AIAA Paper 2002-5869.

[11] Ren, L., Clarke, J. P., and Tan Ho, N., "Achieving Low Approach Noise Without Sacrificing Capacity," *Proceedings of the 22nd Digital Avionics Systems Conference*, Vol. 1, Institute of Electrical and Electronics Engineers, Piscataway, NJ, 2003, pp. 1–9.

[12] Clarke, J. P., Tan Ho, N., Ren, L., Brown, J. A., Elmer, K. R., Tong, K.,

and Wat, J. K., "Continuous Descent Approach: Design and Flight Test for Louisville International Airport," *Journal of Aircraft*, Vol. 41, No. 5, 2004, pp. 1054–1066.

[13] Ren, L., Clarke, J. P., and Tan Ho, N., "Workstation Based Fast-Time Aircraft Simulator for Noise Abatement Approach Procedure Study," AIAA Paper 2004-6503, 2004.

[14] in 't Veld, A. C., van Paassen, M. M., Mulder, M., and Clarke, J. P., "Pilot Support for Separation Assurance during Decelerating Approaches," *Proceedings of the AIAA Guidance, Navigation and Control Conference & Exhibit*, AIAA, Reston, VA, 2005, pp. 1–13; also AIAA Paper 2004-2051.

[15] De Prins, J. L., Schippers, K. F. M., Mulder, M., van Paassen, M. M., in 't Veld, A. C., and Clarke, J. P., "Enhanced Self-Spacing Algorithm for Three-Degree Decelerating Approaches," AIAA 2005-6140, 2005.

[16] Schippers, K. F. M., De Prins, J. L., Mulder, M., van Paassen, M. M., in 't Veld, A. C., and Clarke, J. P., "Investigation of a Three-Degree Decelerating Approach of a Twin Engined Jet Aircraft," AIAA Paper 2005-6139, 2005.

[17] Slater, G. L., "Dynamics of Self-Spacing in a Stream of In-Trail Aircraft," AIAA Paper 2002-4927, 2002.

[18] Moninger, W. R., Mamrosh, R. D., and Pauley, P. M., "Automated Meteorological Reports from Commercial Aircraft," World Meteorological Society, TR ARP 5430, 2003.

[19] Neumaier, A., and Schneider, T., "Estimation of Parameters and Eigenmodes of Multivariate Autoregressive Models," *ACM Transactions on Mathematical Software*, Vol. 27, No. 1, 2001, pp. 27–57.

[20] Tan Ho, N., "Design of Aircraft Noise Abatement Approach Procedures for Near-Term Implementation," Ph.D. Dissertation, Massachusetts Institute of Technology, Department of Aeronautics and Astronautics, 2005.

[21] Hart, S. G., and Staveland, L. E., "Development of NASA-TLX (Task Load Index): Results of Empirical and Theoretical Research," *Human Mental Workload*, edited by P. A. Hancock and N. Meshkati, Elsevier Science Publishers, Amsterdam, 1988, pp. 139–183.